

Nonlinear cosmological structure with ultra-light bosons via modified gravity

Stefany G. Medellín-González* and L. Arturo Ureña-López†

Departamento de Física, DCI, Campus León, Universidad de Guanajuato, 37150, León, Guanajuato, México.

Alma X. González-Morales‡

Consejo Nacional de Ciencia y Tecnología, Av. Insurgentes Sur 1582. Colonia Crédito Constructor, Del. Benito Juárez C.P. 03940, México D.F. México and

Departamento de Física, DCI, Campus León, Universidad de Guanajuato, 37150, León, Guanajuato, México.

(Dated: October 28, 2020)

Ultra-light bosons as dark matter has become a model of major interest in Cosmology, due to the possible imprint of a distinct signature in the cosmic structure both at the linear and non-linear scales. In this work we show that the equations of motion for density perturbations for this kind of models can be written in terms of a modified gravitational potential. Taking advantage of this parallelism, we use the MG-PICOLA code originally developed for modified gravity models to evolve the density field of axion models with and without self-interaction. Our results indicate that the quantum potential adds extra suppression of power at the non-linear level, and it is even capable of smoothing any bumpy features initially present in the mass power spectrum.

I. INTRODUCTION

The existence of dark matter (DM) in the Universe is one of the most challenging puzzles of modern Cosmology[1] and more so because it has been difficult to determine its intrinsic properties beyond the assumption of a pressureless fluid made of massive particles. It is then no surprise that one alternative model, to the so-called Cold Dark Matter, has captured the attention of the community in recent years[2–6], mostly because of the intriguing possibility that the quantum properties of its constituent particles could have been imprinted in the features of galaxies and large scale structure in the Cosmos. The model has been known by different names in the literature, and then we will refer to it indistinctly as scalar field dark matter (SFDM)[7], fuzzy dark matter (FDM)[8], or ultra-light axions[5].

As a direct detection of this kind of particle seems to be beyond the reach of our present technological capabilities[9–12], we must rely on cosmological (i.e. gravitational) observations as the best option to test its existence (eg. [13, 14]). So far, the cosmological evolution is well understood up to the level of linear perturbations, with even dedicated versions of the leading Boltzmann codes that allow a precise comparison of the model with a full suite of cosmological observations[15–18]. However, the nonlinear formation of structure still is a difficult task, and it has been until recently that full simulations seem to be at hand for a proper study of the formation of structure under axion models[19–23]. Although this will allow the systematic testing of the model in the near future, it is necessary to find options for the generation of rapid cosmological simulations much in the same way

as it has been done for Cold Dark Matter (CDM) and Modified Gravity models[24–27].

In this paper we explore such possibility for axion models and argue that, given the scale-dependent growth of density perturbations in these types of models we can use the numerical code MG-PICOLA¹[26], originally developed for MG models. We will do this for the standard FDM model, with its distinctive cut-off in the linear MPS, and also for the so-called extreme axion model[16, 28, 29] that features an excess of power, when compared to CDM, in the growth of linear density perturbations. A key intermediate step in the calculations will be the transformation of the axion field equations into their hydrodynamic counterpart in terms of the well-known Madelung transformation.

A summary of the paper is as follows. In Sec. II we present the main equations of motion for axion models in the non-relativistic limit, and correspondingly their final form in terms of hydrodynamic quantities. We will also explain the expected growth of linear density perturbations and the corresponding appearance of two characteristic length scales (wavenumbers) related to the physical parameters in the model. From here we write the growth factors that describe the evolution of density perturbations up to the second order in Lagrangian dynamics, and how their equations of motion are modified to include the so-called quantum pressure that arises because of the wave properties of axion dark matter. These results will be used in the recently developed Comoving Lagrangian Acceleration (COLA)[30] method in the form developed in MG-PICOLA[26] for scale-dependent models (see also[27, 31]).

In Sec. III we describe the cosmological simulations that are obtained from the theoretical framework of Sec. II, and for different cosmological setups in terms of

* stefany@ugto.mx

† lurena@ugto.mx

‡ alma.gonzalez@fisica.ugto.mx

¹ <https://github.com/HAWinther/MG-PICOLA-PUBLIC>

initial conditions and evolution equations, so that we can determine the main contributions to the non-linear evolution of density perturbations of the axion models. The initial conditions consider the usual FDM suppression of power at small scales, but we also include the possibility for the extreme case in which there is an excess of power as compared to the CDM case. Finally, in Sec. IV we discuss the main results and future perspectives of this work.

II. MATHEMATICAL BACKGROUND

The equations of motion of ultra-light axions in the non-relativistic approximation have been obtained before in Refs. [31–37], and here we will give a brief description of the method. Let us start with the following action,

$$S = \int \sqrt{-g} d^4x \left[\frac{R}{2\kappa^2} + \partial_\mu \phi \partial^\mu \phi^* + \tilde{m}_a^2 |\phi|^2 + \tilde{\lambda} |\phi|^4 \right], \quad (1)$$

where $g = \det(g_{\mu\nu})$, $\kappa^2 = 8\pi G/c^4$, G is Newton's gravitational constant, c is the speed of light, R is the Ricci scalar and ϕ is a complex scalar field endowed with a potential that contains quadratic and quartic interactions terms.²

The parameters in the potential are explicitly given by $\tilde{m}_a = m_a c/\hbar$ and $\tilde{\lambda} = \lambda/(\hbar c)$, where \hbar is the Planck's constant, m is the boson mass and λ is a dimensionless parameter. Notice that the fundamental constants will be shown explicitly, and that the potential parameters become the bare ones if we choose to use natural units $c = \hbar = 1$, i.e. $\tilde{m}_a = m_a$ and $\tilde{\lambda} = \lambda$.³ Notice that the Compton length of the boson particle is just $L_C = 1/\tilde{m}_a$, and correspondingly the Compton time is defined as $T_C = L_C/c$, which is the one used in the field transformation that leads to Eqs. (2).

For the non-relativistic limit (for details see [33, 35–39]), we now apply the field transformation $\phi(t, \mathbf{r}) = e^{i\tilde{m}_a c t} \psi(t, \mathbf{r})$, where the new field ψ will obey the conditions that the order of magnitude of the field derivatives are $\partial_t \psi \sim \partial_r^2 \psi = \mathcal{O}(\epsilon^2)$, with $|\epsilon| \ll 1$. Additionally, we consider a perturbed FRW metric in the form $ds^2 = -(1 + 2\Psi/c^2)dt^2 + a^2(t)(1 - 2\Psi/c^2)d\mathbf{x}^2$, where Ψ is the Newtonian gravitational potential and $a = a(t)$ is the scale factor of the Universe. Thus, the equations of motion derived from the action (1) can be written in the

form of the well-known Gross-Pitaevskii-Poisson (GPP) system,

$$i\hbar \frac{\partial_t(a^{3/2}\psi)}{a^{3/2}} = -\frac{\hbar c}{2\tilde{m}_a a^2} \nabla^2 \psi + \left(\frac{\Psi}{c^2} + \frac{\tilde{\lambda}}{2\tilde{m}_a^2} |\psi|^2 \right) \tilde{m}_a \psi, \quad (2a)$$

$$\nabla^2 \Psi = \frac{4\pi G}{c^2} a^2 \tilde{m}_a^2 |\psi|^2 \left(1 + \frac{\tilde{\lambda}}{2\tilde{m}_a^2} |\psi|^2 \right) - \frac{3}{2} a^2 H^2, \quad (2b)$$

where H is the Hubble parameter. Eqs. (2) are complemented by the Friedmann constraint $H^2 = (8\pi G/c^2)\rho_b$, being ρ_b the background (homogeneous) density.

One note is in turn regarding the quadratic terms in Eqs. (2), which come from the quartic field term in the action (1). As shown in a variety of previous works[40, 41], the quartic term changes the early-time behavior of the scalar field, as the latter is not pressureless anymore. Hence, one comes to the general conclusion that the quadratic terms in Eqs. (2) should become small before the expected time of radiation-matter equality. In other words, once the scalar field behaves as pressureless matter, we find that $(\tilde{\lambda}/2\tilde{m}_a^2)|\psi|^2 \ll 1$, and then we will hereafter drop such term from Eq. (2b).

We now apply the Madelung transformation in the form $\tilde{m}_a \psi = c\sqrt{\rho(t, \mathbf{x})} e^{iS(t, \mathbf{x})/\hbar}$, where $\rho(t, \mathbf{x})$ is the density field and $\mathbf{u} = \nabla S/m_a$ is the velocity field, which is then irrotational by definition, $\nabla \times \mathbf{u} = 0$. It must be noted that in doing the Madelung transformation we are assuming that the non-relativistic matter density is strictly given by $\rho = \tilde{m}_a^2 |\psi|^2/c^2$. The GPP system (2) then becomes the Quantum Barotropic Euler-Poisson (QBEP) one[20, 21, 31, 38, 42, 43], which we write in the form

$$\frac{\partial \rho}{\partial t} + 3H\rho + \frac{1}{a^2} \nabla \cdot (\rho \mathbf{u}) = 0, \quad (3a)$$

$$\frac{\partial \mathbf{u}}{\partial t} + (\mathbf{u} \cdot \nabla) \mathbf{u} = -\nabla \tilde{\Psi}, \quad (3b)$$

$$\nabla^2 \tilde{\Psi} = 4\pi G a^2 \delta \rho + \frac{\tilde{\lambda} c^4}{2\tilde{m}_a^4} \nabla^2 \rho - \frac{c^2}{2\tilde{m}_a^2 a^2} \nabla^2 \left(\frac{\nabla^2 \sqrt{\rho}}{\sqrt{\rho}} \right), \quad (3c)$$

where $\delta \rho = \rho - \rho_b$. To serve our purposes, we have written the force on the right hand side of Eq. (3b) in terms of the gradient of an effective potential $\tilde{\Psi}$, whose corresponding Poisson equation is sourced by a combination of linear and nonlinear functions of the matter density ρ , the last of which is called the quantum potential.

It is convenient to write Eqs. (3) in terms of the density contrast $\delta(t, \mathbf{x}) = \rho(t, \mathbf{x})/\rho_b - 1$, whereas for the velocity we take $\mathbf{u} = H\mathbf{r} + \mathbf{v}$, with \mathbf{v} the peculiar velocity. As is well known from the theory of linear density perturbations, corresponding to $|\delta| \ll 1$ and $|\mathbf{v}| \ll 1$, Eqs. (3) can be combined into a single one for the density contrast in the form

$$\ddot{\delta} = 4\pi G \rho_b a^4 \delta + \frac{\tilde{\lambda} c^4 \rho_b a^2}{\tilde{m}_a^4} \nabla^2 \delta - \frac{c^2}{4\tilde{m}_a^2} \nabla^2 (\nabla^2 \delta), \quad (4)$$

where a dot means derivative with respect to the so-called superconformal time τ defined through the relation $a^2 d\tau = dt$.

² Although there are some differences between real and complex scalar fields at the relativistic level, their non-relativistic dynamics, which is our regime of physical interest, is driven by the same set of equations. Thus, all results presented here apply for both the real and complex cases.

³ Under our convention the units of the different physical quantities are as follows: $[\phi] = [\psi] = (\text{energy}/\text{length})^{1/2}$, $[\tilde{m}_a] = \text{length}^{-1}$ and $[\tilde{\lambda}] = (\text{energy} \cdot \text{length})^{-1}$. With this Planck's constant \hbar will not appear explicitly in Eqs. (3) below. In natural units we find that: $[\phi] = \text{energy}$, $[\tilde{m}_a] = \text{energy}$ and $\tilde{\lambda}$ becomes dimensionless.

Thus, the equation of motion (4) at linear order for a given Fourier mode of the density contrast δ_k , with corresponding wavenumber k , reads

$$\ddot{\delta}_k = 4\pi G\rho_b a^4 \mu(a, k, \tilde{\lambda}) \delta_k, \quad (5a)$$

where[33]

$$\mu(a, k, \tilde{\lambda}) = 1 - k^2/k_{J1}^2 - k^4/k_{J0}^4. \quad (5b)$$

In the foregoing equation, we have implicitly defined the Jeans wavenumber of FDM as: $k_{J0}^4 = (16\pi G/c^2)\rho_b a^4 \tilde{m}_a^2$. Also, we have defined a second characteristic wavenumber as: $k_{J1}^2 = (4\pi G/c^4)a^2 \tilde{m}_a^4/\tilde{\lambda}$. For reference, the CDM case corresponds to $\mu(a, k, \tilde{\lambda}) = 1$.

The first Jeans wavenumber can be written as [5, 8, 16],

$$k_{J0} = 66.5a^{1/4} \left(\frac{\tilde{m}_a}{10^{-22}\text{eV}} \right)^{1/2} \left(\frac{\Omega_{a0} h^2}{0.12} \right)^{1/4} \text{Mpc}^{-1}. \quad (6)$$

The influence of k_{J0} in the evolution of density perturbations changes with time, and some level of suppression of the perturbations, in comparison with CDM, is expected for scales in the range $k \gtrsim 10 h\text{Mpc}^{-1}$ ever since the time of radiation-matter equality.

Likewise, the effects from the second instability scale k_{J1} on the growth of density perturbations are only present at early times. One must recall that the second term on the rhs of Eq. (4) is related to the quartic term in the Schrodinger equation (2a), and then we also find $(\tilde{\lambda}/2\tilde{m}_a^2)|\psi|^2 = (\tilde{\lambda}c^2/2\tilde{m}_a^4)\rho_b \ll 1$ after the time of radiation-matter equality. The main conclusion here is that any effects from the second Jeans wavenumber k_{J1} can be studied in terms of the fluid equations of the FDM case ($\tilde{\lambda} = 0$), as long as the initial conditions already take into account the effects of the SF self-interaction on the linear MPS. Because of this, we will hereafter consider $\tilde{\lambda} = 0$ in all expressions regarding the evolution of density perturbations.

Our next step is to study the nonlinear stage of structure formation, and for that, we resort to the scale-dependent COLA method of[26]. We first assume that the equation of motion of the particles in an N -body simulation is $\ddot{\mathbf{x}} = -\nabla\tilde{\Psi}$, where $\tilde{\Psi}$ is the potential in Eqs. (3). From this we obtain a scale-dependent, first order, growth factor $D_1(\tau, k)$ that obeys the equation

$$\ddot{D}_1 - 4\pi G\rho_b a^4 \mu(a, k) D_1 = 0. \quad (7a)$$

A second order growth factor $D_2(\tau, k)$ is also obtained by simply relying on the expressions developed in[26] (see their Eq. (4.10)) for modified gravity models, namely,

$$\ddot{D}_2 - 4\pi G\rho_b a^4 \mu(a, k) D_2 = -D_1^2 [4\pi G\rho_b a^4 \mu(a, k) + 2a^4 H^2 \gamma_2(\mathbf{k}, \mathbf{k}_1, \mathbf{k}_2, a)], \quad (7b)$$

where

$$\gamma_2(\mathbf{k}, \mathbf{k}_1, \mathbf{k}_2, a) = \gamma_2^E(\mathbf{k}, \mathbf{k}_1, \mathbf{k}_2, a) + \frac{3\mathbf{k}_1 \cdot \mathbf{k}_2}{4k_1^2 k_2^2} \Omega_b(a) [(\mu(a, k) - \mu(a, k_1))k_1^2 + (\mu(a, k) - \mu(a, k_2))k_2^2], \quad (7c)$$

Here, \mathbf{k}_1 and \mathbf{k}_2 are wavevectors in Fourier space that must comply with the triangle constraint $\mathbf{k} = \mathbf{k}_1 + \mathbf{k}_2$.

To find γ_2^E we require an expansion up to second order

of $\nabla^2\tilde{\Psi}$ in Fourier space. In configuration space, we find for the third term on the right-hand side of Eq. (3c),

$$\nabla^2 \left(\frac{\nabla^2 \sqrt{1+\delta}}{\sqrt{1+\delta}} \right) = \frac{1}{2} \nabla^2 (\nabla^2 \delta) - \frac{1}{8} \nabla^2 (\nabla^2 \delta^2) - \frac{1}{4} (\nabla^2 \delta)^2 - \frac{1}{2} \nabla \delta \cdot \nabla (\nabla^2 \delta) - \frac{1}{4} \delta \nabla^2 (\nabla^2 \delta) + \mathcal{O}(\delta^3). \quad (8)$$

Following the notation of[26, 31], the second order kernel γ_2^E obtained from the Fourier transform of Eq. (8) is

$$\gamma_2^E = \frac{c^2}{8a^4 H^2 \tilde{m}_a^2} (k_1^2 + k_2^2 + \mathbf{k}_1 \cdot \mathbf{k}_2) (\mathbf{k}_1 + \mathbf{k}_2)^2. \quad (9)$$

III. COSMOLOGICAL SIMULATIONS

To study the nonlinear evolution of density perturbations, we then use the code `MG-PICOLA`[26] supplied with the MG functions $\mu(a, k)$ and $\gamma_2^E(a, k)$ described above. But before we describe the main results, there are a couple of pertinent notes about the numerical calculations in the code.

The first one is related to the solution of the Fourier

integrals. To enhance the speed of the calculations in Fourier space, MG-PICOLA takes by default the orthogonal triangle configuration $\mathbf{k}_1 \cdot \mathbf{k}_2 = 0$ and $k_1 = k_2 = k/\sqrt{2}$ [26]. This is the same choice considered in our simulations, under which we find from Eq. (7c) that $\gamma_2 = \gamma_2^E = c^2 k^4 / (8a^4 H^2 \tilde{m}_a^2)$. The latter implies that the second term on the right-hand side of Eq. (7b) contributes with the same factor as that of the Jeans wavenumber in the first term, but with the opposite sign. The overall result is then that the equation of motion of the second growth factor (7b) simplifies to

$$\ddot{D}_2 - 4\pi G \rho_b a^4 \mu(a, k) D_2 = -4\pi G \rho_b a^4 D_1^2. \quad (10)$$

Thus, the only scale-dependent influence on the evolution of D_2 is provided by the term $\mu(a, k)$. It must be stressed out that this result arises directly from both the nature of the SFDM model and the approximation to increase the speed of MG-PICOLA. Other approximations, like the so-called equilateral ($k_1 = k_2 = k$ and $\mathbf{k}_1 \cdot \mathbf{k}_2 = 1/2$) or squeezed ($k_1 = k$, $k_2 \simeq 0$ and $\mathbf{k}_1 \cdot \mathbf{k}_2 \simeq 0$) ones, may allow for more scale-dependent effects in the evolution of D_2 . However, as argued in [26], it is expected that the orthogonal approximation already takes into account most of the weight arising from the Fourier integrals.

The second one is about the initial conditions for the growth factors. Once supplied with a linear MPS of the desired model at the initial redshift z_i , the code evolves the growth factors D_1 and D_2 , by means of Eqs. (7), up to the present time using the initial conditions $D_1(z_i, k) = 1$, $\dot{D}_1(z_i, k) = \mathcal{H}_i$, $D_2(z_i, k) = -3/7$ and $\dot{D}_2(z_i, k) = -(6/7)\mathcal{H}_i$, where $\mathcal{H} = \dot{a}/a$. The resultant growth factors are then normalized so that their values at $z = 0$ is unity, that is, $D_1(0, k) = 1 = D_2(0, k)$. This is a convenient procedure for the CDM case, for which the growth factors are scale independent, and then the normalization at $z = 0$ translates into the same initial conditions at z_i for all scales.

For models with scale-dependent growth factors, as our model of interest, the normalization to unity at $z = 0$ means that the initial conditions at z_i are not the same for all scales, but that the initial amplitudes of $D_1(z_i, k)$ and $D_2(z_i, k)$ would be artificially deformed and may not be the correct ones corresponding to the scale-dependent model under consideration. To minimize the deformation of the initial conditions, we have instead normalize the growth factors with respect to their values at large scales, ie $D_1^{new}(z, k) = D_1(z, k)/D_1(0, k \rightarrow 0)$ and $D_2^{new}(z, k) = D_2(z, k)/D_2(0, k \rightarrow 0)$. As our model has the same perturbations at large scales as CDM, the normalization factors are also the same obtained from a CDM simulation, that is, $D_1(0, k \rightarrow 0) = D_1^{CDM}(0)$ and $D_2(0, k \rightarrow 0) = D_2^{CDM}(0)$. In this form, the initial conditions will be the same for all scales, as we readily find that $D_1^{new}(z_i, k) = 1/D_1(0, k \rightarrow 0)$ and $D_2^{new}(z_i, k) = -3/(7D_2(0, k \rightarrow 0))$, and any scale-dependent power suppression is left encoded intact in the initial MPS.

We performed a series of tests to assure the convergence of the numerical results, and from them, we selected the optimal parameters for the number of particles, number of mesh points, time steps, box size and the initial redshift of the simulations. Following the labeling in [21, 44] for cosmological simulations, we studied the following cases: CIC (Cold Initial Conditions)⁴, that corresponds to a typical CDM simulation; FIC (Fuzzy Initial Conditions), that corresponds to a CDM simulation plus initial conditions from FDM; and FIC+QP, for which we additionally activated the modified-gravity functions in MG-PICOLA to take into account the effects from the quantum potential Q .

The main characteristics of our simulations are summarized in Table I. We use a fiducial boson mass of $m_a = 10^{-23}$ eV/ c^2 and 800 COLA steps for the FIC, FIC+QP and EIC+QP simulations, in order to make sure the effects of the quantum terms for the range of wavenumbers contained in our simulations boxes are well resolved, notice that the Nyquist scale is at $k_{\text{Nyquist}} \simeq 214h/\text{Mpc}$. Additionally, our simulations were started at $z = 30$ for the FIC and FIC+QP, and at $z = 100$ for the EIC one, to assure the compatibility of the initial conditions with those of linear perturbations, which were obtained with an amended version of the Boltzmann code CLASS (v2.7)[16] (see also [18] for a comparison of our formalism in solving the field equations with other approaches). The main quantity we use as a comparison between simulations is the MPS measured using the particles, which is shown in Fig. 1 below for different redshift $z = 30, 5, 2.5$ and for each simulation.

In the top panel of Fig. 1 we see a comparison between the simulations CIC, which is the standard CDM one, and FIC+QP, which considers both initial conditions and evolution of the FDM type. The initial MPS at $z = 30$ for the latter shows the characteristic drop in power at small scales (for $k \gtrsim 2\text{Mpc}/h$) although a comparison with the linear MPS obtained directly from CLASS shows that the oscillations have been smoothed out by MG-PICOLA. Nonetheless, we see that the MPS of the FIC+QP simulation remains suppressed, at small scales, up to $z = 5$, with respect to that of the CIC simulation, although the difference between the two is almost lost by $z = 2.5$, being the relative difference of about 10% at most.

We see in the FIC+QP simulations a transfer of power from large to small scales, an effect that has been widely reported in similar simulations of the FDM model, although only for those that exploit the similarity with the hydrodynamic equations via the Madelung transformation. However, we consider the evolution of the MPS to be trusted only up to $k \simeq 7.5h\text{Mpc}^{-1}$ (vertical dot-dashed line), which is set by the scale at which the initial MPS is above the shot-noise one (slopping dot-dashed

⁴ Not to confuse with the standard notation CIC that stands for Cloud In Cell.

TABLE I. Parameter specification for the cosmological simulations described in the text. The Nyquist wavenumber for this setup is given by $k_{\text{Nyquist}} \simeq 214 h/\text{Mpc}$. The initial redshift for the CIC, FIC and FIC+QP is $z = 30$, while for the EIC+QP is $z = 100$. See the text for a discussion on the later case.

| Type | Model | Initial Conditions | $m_a c^2$ [eV] | N_{part} | Boxsize [Mpc/h] |
|----------|---------------|--------------------|---------------------|-------------------|-----------------|
| CIC | Λ CDM | CDM | - | 1024^3 | 15 |
| FIC | Λ CDM | FDM | 3×10^{-23} | 1024^3 | 15 |
| FIC + QP | Λ FDM | FDM | 3×10^{-23} | 1024^3 | 15 |
| EIC + QP | Λ FDM | EFDM | 3×10^{-23} | 1024^3 | 15 |

line). Even though it is known that for Particle-Mesh like codes the effect of shot-noise affects less the evolution of models with suppression in the MPS [45], we have preferred to be conservative. The sub-panel in this figure shows the relative difference between MPS measured in the CIC and FIC+QP, which we can notice diminishes with the redshift evolution.

It should also be recalled that the Jeans length k_{J0} is evolving, but for the parameters in our simulation its variation, from $z_i = 30$ up to the present, is in the range (see for instance [5, 16])

$$13 h\text{Mpc}^{-1} \lesssim k_{J0} \lesssim 30 h\text{Mpc}^{-1}. \quad (11)$$

This means that the SFDM density contrast, and in turn the MPS, is evolving like CDM for the range of wavenumbers considered in Fig. 1, given that for them we obtain $\mu(a, k) \simeq 1$ for all practical purposes.

As for the bottom panel of Fig. 1, we see a comparison between the FIC and FIC+QP simulations, to see the influence of the quantum potential term (see the last term on the right-hand side in Eq. (3c)) in the evolution of the MPS. The initial MPS is the same for both simulations, and the relative difference is marginal afterwards, with a relative difference of about 0.25% at most, with the MPS from the FIC+QP simulation consistently suppressed throughout the evolution, which we consider an effect of the quantum pressure (as suggested by the accompanying lower panel which shows the fractional difference between the two cases). In overall, this comparison reinforces our statement above in that the inclusion of the quantum pressure gives marginal differences in the evolution of FDM density perturbations.

Finally, in Fig. 2 we show the comparison between the CDM and EIC+QP simulations, the latter corresponding to the model with power enhancement at small scales. Here, the acronym EIC+QP means extreme initial conditions plus the quantum force, where extreme refers to the standard axion case and the reported excess of power in density perturbations reported in [15, 16, 44]. As explained in [15, 16], the axion case can be approximated by the action (1) but with a negative self-interaction parameter, $\tilde{\lambda} < 0$.

We can also consider such a case given that the excess of power must be imprinted on the MPS around the time the scalar field behaves as a pressureless matter, which happens before the time of radiation-matter equality if $\tilde{m}_a > 10^{-25}$ eV [16]. Thus, the only effect

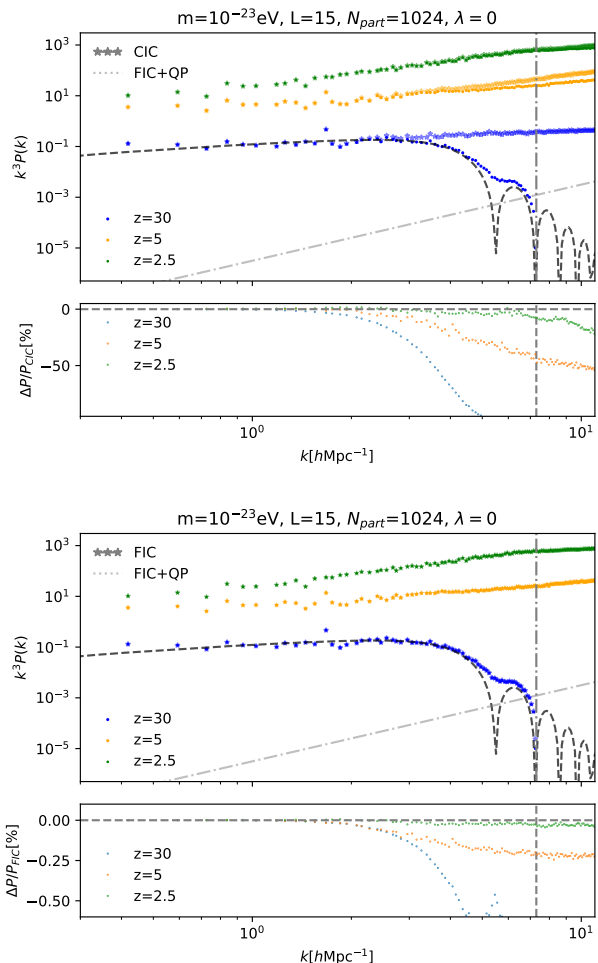


FIG. 1. (Top Figure) Comparison of the measured particle MPS for the CIC (stars) and FIC+QP (dots) at different redshift, $z = 30$ (blue), $z = 5$ (yellow) and $z = 2.5$ (yellow). The linear MPS from CLASS, used as initial condition, is shown for comparison (dashed black line). The lower sub-panel shows the relative difference between the cases considered, for the three redshifts: $\Delta P/P_{\text{CIC}} = (P_{\text{FIC+QP}} - P_{\text{CIC}})/P_{\text{CIC}}$. Notice that the relative difference decreases for lower redshift. We also show for reference the wavenumber for which the initial MPS is below the shot-noise (vertical dot-dashed gray line) and the amplitude of the shot-noise (sloping dot-dashed gray line), in order to delimit the k range that could be influenced by shot-noise. (Lower Figure) Same as the Top figure but the comparison is with respect to the FIC simulation.

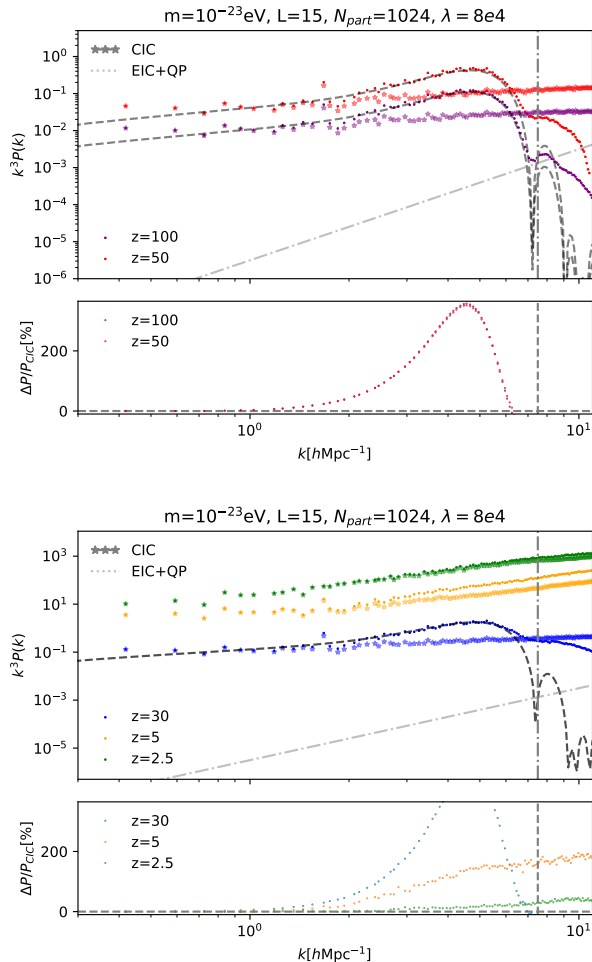


FIG. 2. (Top Figure) Comparison of the measured particle MPS for the CIC (stars) and EIC+QP (dots) at different redshift, $z = 100$ (purple) and $z=50$ (red). See details of the simulation boxes in Table I. The linear MPS from CLASS, used as initial condition, is shown for comparison (dashed black line). The lower sub-panel shows the relative difference between the cases considered, for the two redshifts: $\Delta P/P_{\text{CIC}} = (P_{\text{EIC+QP}} - P_{\text{CIC}})/P_{\text{CIC}}$. Notice that the relative difference decreases for lower redshift. We also show for reference the wavenumber for which the initial MPS is below the shot-noise (vertical dot-dashed gray line) and the amplitude of the shot-noise (sloping dot-dashed gray line), in order to delimit the k range that could be influenced by shot-noise. (Lower Figure) Same as the Top figure but the comparison is for the low redshifts $z = 30$ (blue), $z = 5$ (yellow) and $z = 2.5$ (green).

that is still present at late times is the suppression of the MPS at small scales due to the quantum potential term in Eq. (3c). In other words, EIC+QP means that the initial MPS has an excess of power with respect to CDM and that density perturbations are evolved by the same dynamics as the FDM model.

The EIC+QP case shown in Fig. 2 considers that the decay constant of the axion field f_a is such that

$8\pi G f_a / c^2 \simeq 1.25 \times 10^{-5}$, and the initial MPS was calculated as explained in [15, 16]. We can see that at $z = 100$ there is already an excess of power with respect to CDM at around $k \simeq 7 h\text{Mpc}^{-1}$, and also a typical suppression of power for larger wavenumbers (smaller scales).

As mentioned before for the previous cases, the initial MPS calculated by MG-PICOLA appears to be smoothed out with respect to that obtained from CLASS, but otherwise they agree very well. However, we can see that by $z = 30$ there appears a noticeable difference in the MPS calculated from the two codes: the one from MG-PICOLA shows a less pronounced suppression of power at small scales. This result is in stark contrast to the cases in Fig. 1, for which the agreement between the two MPS is very good at $z = 30$. Such result can be explained in terms of the transfer of power from large to small scales, due to the presence of the power excess in the initial MPS, but such transfer seems to happen from a much earlier time.

A similar effect was studied before in [46] for artificially induced peaks in the initial MPS: the nonlinear MPS obtained from N-body simulations shows that power from large scales is transferred evenly to small scales. In our case, which in addition to a peak has a suppression of power at small scales, such effect means that the nonlinear MPS in the EIC+QP case should show an excess of power at small scales as compared to the standard FIC case.

IV. CONCLUSIONS AND DISCUSSION

There are some limitations in our approach to SFDM simulations. The first one is that in the calculation of the scale-dependent corrections to the evolution of the first and second order growth factors, we had to rely on perturbative expansions in terms of δ for the effective quantum potential. Such expansion is formally valid for small amplitudes $|\delta| \lesssim 1$, and then is not reliable for the highly non-linear regime of density perturbations. This is a limitation of the SFDM model only, as for Modified Gravity models the scale-dependent corrections are directly proportional to the density contrast δ by definition and then all calculations are applicable to both the linear and non-linear regimes.

Nonetheless, our results are to be trusted up to second order in δ , specially because the second order corrections were canceled by the particular approximation of orthogonal triangle configurations in Fourier space. This is a favorable coincidence that helped us to have more reliable results at least at the level of 2LPT.

One general result in our simulations is the transfer of power from large to small scales, as seen in the calculated MPS, which means that the characteristic suppression of power is no longer as acute as in the linear evolution, although we were able to quantify a visible difference with respect to CDM even at small redshifts. It should be noted that our numerical simulations do not show any

major difference in the aforementioned transfer of power in the cases we use what we called the CDM and FDM evolution (FIC and FIC+QP simulations, respectively), and then the final profile of the MPS is the same for all practical purposes up to redshift $z = 2.5$.

We also presented the results corresponding to the extreme axion case (EIC+QP), with its characteristic excess of power in the MPS. Here our simulations indicate also a convergence of the MPS towards the CDM one by means of transfer of power from large to small scales, although the MPS remains overpowered as compared to CDM.

It is important to mention that although it is well known that for models with suppression in the MPS the effect of the shot-noise can be important, it is also known that Particle-Mesh like techniques are less affected [45]. Nevertheless, in order to use this type of simulations for larger axion mass values, which are of higher interest

given current constraints, it would require us to make a deeper study of the effect of the noise.

ACKNOWLEDGMENTS

We are thankful to Jorge Cervantes-Cota and Alejandro Avilés for useful conversations and clarifications on the scale-dependent COLA method, and to Octavio Valenzuela for the discussion of the results from the simulations perspective. SGM-G thanks CONACYT for financial support. AXGM acknowledges support from Cátedras CONACYT. This work was partially supported by Programa para el Desarrollo Profesional Docente; Dirección de Apoyo a la Investigación y al Posgrado, Universidad de Guanajuato, research Grants No. 036/2020, 099/2020; CONACyT México under Grants No. A1-S-17899, 286897, 297771,304001; and the Instituto Avanzado de Cosmología Collaboration.

-
- [1] L. Baudis, (2018), arXiv:arXiv:1801.08128v1.
- [2] J. C. Niemeyer, (2019), arXiv:1912.07064 [astro-ph.CO].
- [3] L. A. Ureña-López, *Front. Astron. Space Sci.* **6**, 47 (2019).
- [4] L. Hui, J. P. Ostriker, S. Tremaine, and E. Witten, *Physical Review D* **95**, 043541 (2017), arXiv:1610.08297.
- [5] D. J. Marsh, *Physics Reports* **643**, 1 (2016), arXiv:1510.07633.
- [6] J. Magaña, T. Matos, V. Robles, and A. Suárez, , 1 (2012), arXiv:1201.6107; J. Magaña, T. Matos, A. Suárez, and F. Sánchez-Salcedo, *Journal of Cosmology and Astroparticle Physics* **2012**, 003 (2012), arXiv:1204.5255.
- [7] T. Matos, F. S. Guzmán, and L. A. Ureña-López, *Classical and Quantum Gravity* **17**, 1707 (2000), arXiv:9908152 [astro-ph]; T. Matos and L. Arturo Ureña-López, *Physical Review D* **63**, 063506 (2001), arXiv:0006024 [astro-ph]; T. Matos and L. A. Ureña-López, *Classical and Quantum Gravity* **17**, 1 (2000), arXiv:0004332v2 [arXiv:astro-ph].
- [8] W. Hu, R. Barkana, and A. Gruzinov, *Physical Review Letters* **85**, 1158 (2000), arXiv:0003365 [astro-ph].
- [9] J. Manley, R. Stump, D. Wilson, D. Grin, and S. Singh, (2019), arXiv:1910.07574 [astro-ph.IM].
- [10] T. Emken and C. Kouvaris, , 29 (2018), arXiv:1802.04764.
- [11] E. Aprile *et al.*, *Physical Review Letters* **119**, 6 (2017), arXiv:1705.06655.
- [12] X. Cui *et al.*, *Physical Review Letters* **119**, 1 (2017), arXiv:1708.06917.
- [13] D. Grin, M. A. Amin, V. Gluscevic, R. Hložek, D. J. E. Marsh, V. Poulin, C. Prescod-Weinstein, and T. L. Smith, (2019), arXiv:1904.09003 [astro-ph.CO].
- [14] V. Poulin, T. L. Smith, D. Grin, T. Karwal, and M. Kamionkowski, *Phys. Rev.* **D98**, 083525 (2018), arXiv:1806.10608 [astro-ph.CO].
- [15] F. X. L. Cedeño, A. X. González-Morales, and L. A. Ureña-López, “Ultralight dm bosons with an axion-like potential: scale-dependent constraints revisited,” (2020), arXiv:2006.05037 [astro-ph.CO].
- [16] F. X. Cedeño, A. X. González-Morales, and L. A. Ureña-López, *Physical Review D* **96**, 1 (2017), arXiv:1703.10180; L. A. Ureña-López and A. X. Gonzalez-Morales, *Journal of Cosmology and Astroparticle Physics* **2016** (2016), 10.1088/1475-7516/2016/07/048, arXiv:1511.08195.
- [17] R. Hložek, D. J. E. Marsh, and D. Grin, *Mon. Not. Roy. Astron. Soc.* **476**, 3063 (2018), arXiv:1708.05681 [astro-ph.CO]; R. Hložek, D. J. E. Marsh, D. Grin, R. Allison, J. Dunkley, and E. Calabrese, *Phys. Rev.* **D95**, 123511 (2017), arXiv:1607.08208 [astro-ph.CO]; R. Hložek, D. Grin, D. J. E. Marsh, and P. G. Ferreira, *Phys. Rev.* **D91**, 103512 (2015), arXiv:1410.2896 [astro-ph.CO].
- [18] J. Cookmeyer, D. Grin, and T. L. Smith, *Phys. Rev.* **D101**, 023501 (2020), arXiv:1909.11094 [astro-ph.CO].
- [19] B. Schwabe, M. Gosenca, C. Behrens, J. C. Niemeyer, and R. Easther, “Axionyx: Simulating mixed fuzzy and cold dark matter,” (2020), arXiv:2007.08256 [astro-ph.CO].
- [20] P. Mocz *et al.*, (2019), arXiv:1911.05746 [astro-ph.CO]; *Phys. Rev. Lett.* **123**, 141301 (2019), arXiv:1910.01653 [astro-ph.GA]; L. Lancaster, C. Giovanetti, P. Mocz, Y. Kahn, M. Lisanti, and D. N. Spergel, *JCAP* **2001**, 001 (2020), arXiv:1909.06381 [astro-ph.CO]; P. Mocz, L. Lancaster, A. Fialkov, and F. Becerra, (2018), arXiv:1801.03507; P. Mocz, M. Vogelsberger, V. H. Robles, J. Zavala, M. Boylan-Kolchin, A. Fialkov, and L. Hernquist, *Mon. Not. Roy. Astron. Soc.* **471**, 4559 (2017), arXiv:1705.05845 [astro-ph.CO].
- [21] M. Nori and M. Baldi, **17**, 1 (2018), arXiv:1801.08144; M. Nori, R. Murgia, V. Iršič, M. Baldi, and M. Viel, *Mon. Not. Roy. Astron. Soc.* **482**, 3227 (2019), arXiv:1809.09619 [astro-ph.CO].
- [22] H.-Y. Schive, M.-H. Liao, T.-P. Woo, S.-K. Wong, T. Chiueh, T. Broadhurst, and W.-y. P. Hwang, *Physical Review Letters* **113**, 261302 (2014), arXiv:1407.7762.
- [23] T.-P. Woo and T. Chiueh, *The Astrophysical Journal*

- 697**, 850 (2009), arXiv:0806.0232.
- [24] M. Vogelsberger, F. Marinacci, P. Torrey, and E. Puchwein, (2019), arXiv:1909.07976 [astro-ph.GA].
- [25] G. Valogiannis and R. Bean, *Physical Review D* **95**, 1 (2017), arXiv:1612.06469.
- [26] H. A. Winther, K. Koyama, M. Manera, B. S. Wright, and G. B. Zhao, *Journal of Cosmology and Astroparticle Physics* **2017** (2017), 10.1088/1475-7516/2017/08/006, arXiv:1703.00879.
- [27] A. Aviles and J. L. Cervantes-Cota, *Physical Review D* **96**, 123526 (2017), arXiv:1705.10719.
- [28] U.-H. Zhang and T. Chiueh, *Physical Review D* **96**, 063522 (2017), arXiv:1705.01439.
- [29] U.-H. Zhang and T. Chiueh, *Physical Review D* **96**, 023507 (2017), arXiv:1702.07065.
- [30] S. Tassev, M. Zaldarriaga, and D. J. Eisenstein, *Journal of Cosmology and Astroparticle Physics* **2013** (2013), 10.1088/1475-7516/2013/06/036, arXiv:1301.0322.
- [31] B. Bose and K. Koyama, *Journal of Cosmology and Astroparticle Physics* **2016** (2016), 10.1088/1475-7516/2016/08/032, arXiv:1606.02520; A. Suárez and P.-H. Chavanis, , 1 (2017), arXiv:1710.10486.
- [32] A. Suárez and P. H. Chavanis, *Physical Review D* **95**, 1 (2017), arXiv:1608.08624.
- [33] J. Fan, *Physics of the Dark Universe* **14**, 84 (2016), arXiv:1603.06580.
- [34] D. J. Marsh, *Physical Review D* **91**, 123520 (2015), arXiv:1504.00308.
- [35] L. A. Ureña-López, *Physical Review D - Particles, Fields, Gravitation and Cosmology* **90**, 1 (2014), arXiv:1310.8601.
- [36] F. S. Guzmán and L. A. Ureña-López, *Physical Review D* **69**, 1 (2004), arXiv:0404014 [gr-qc].
- [37] E. Seidel and W. M. Suen, *Physical Review D* **42**, 384 (1990).
- [38] P. H. Chavanis, *Physical Review D - Particles, Fields, Gravitation and Cosmology* **84** (2011), 10.1103/PhysRevD.84.063518, arXiv:1103.3219.
- [39] R. Ruffini and S. Bonazzola, *Physical Review* **187**, 1767 (1969).
- [40] B. Li, T. Rindler-Daller, and P. R. Shapiro, *Physical Review D* **89**, 083536 (2013), arXiv:1310.6061.
- [41] S.-C. Lin, H.-Y. Schive, S.-K. Wong, and T. Chiueh, (2018), arXiv:1801.02320.
- [42] T. Matos, “Scalar field dark matter quantum effects as dark energy,” (2009), arXiv:0909.3634 [astro-ph.CO]; P. H. Chavanis, *Astronomy & Astrophysics* **537**, A127 (2012), arXiv:1103.2698; A. Suárez and T. Matos, *Monthly Notices of the Royal Astronomical Society* **000**, no (2011), arXiv:1101.4039.
- [43] M. A. Rodríguez-Meza and A. H.-A. y Tonatiuh Matos, “Materia oscura escalar compleja (parte i): la versión hidrodinámica,” (2017), arXiv:1708.06701 [astro-ph.GA].
- [44] J. Zhang, Y.-L. S. Tsai, J.-L. Kuo, K. Cheung, and M.-C. Chu, *The Astrophysical Journal* **853**, 51 (2018), arXiv:1611.00892.
- [45] R. E. Angulo, O. Hahn, and T. Abel, *Mon. Not. Roy. Astron. Soc.* **434**, 3337 (2013), arXiv:1304.2406 [astro-ph.CO].
- [46] Z. Ma, *The Astrophysical Journal* **665**, 887–898 (2007).